

A Little Bit of Carbon Can do a Lot for Superconductivity in H₃S

Xiaoyu Wang, Tiange Bi, Katerina P. Hilleke

Department of Chemistry, State University of New York at Buffalo, Buffalo, NY 14260-3000, USA

Anmol Lamichhane

Department of Physics, University of Illinois Chicago, Chicago, IL 60607-7059, USA

Russell J. Hemley*

Department of Physics, University of Illinois Chicago, Chicago, IL 60607-7059, USA

Department of Chemistry, University of Illinois Chicago, Chicago, IL 60607-7059, USA

Eva Zurek*

Department of Chemistry, State University of New York at Buffalo, Buffalo, NY 14260-3000, USA

November 16, 2021

Abstract

Recently, room temperature superconductivity was measured in a carbonaceous sulfur hydride material whose identity remains unknown. Herein, first-principles calculations are performed to provide a chemical basis for structural candidates derived by doping H₃S with low levels of carbon. Pressure stabilizes unusual bonding configurations about the carbon atoms, which can be six-fold coordinated as CH₆ entities within the cubic H₃S framework, or four-fold coordinated as methane intercalated into the H-S lattice, with or without an additional hydrogen in the framework. The doping breaks degenerate bands, lowering the density of states at the Fermi level (N_F), and localizing electrons in C-H bonds. Low levels of CH₄ doping do not increase N_F to values as high as those calculated for $Im\bar{3}m$ -H₃S, but they yield a larger logarithmic average phonon frequency, and an electron-phonon coupling parameter comparable to that of $R\bar{3}m$ -H₃S. The implications of carbon doping on the superconducting properties are discussed.

*Correspondence should be addressed to: rhemley@uic.edu; ezurek@buffalo.edu

Introduction

The decades old quest for a room-temperature superconductor has recently come to fruition. Inspired by Ashcroft’s predictions that hydrogen-rich compounds metallized under pressure could be phonon-mediated high-temperature superconductors^{1;2}, synergy between experiment and theory has led to remarkable progress³⁻⁵. A superconducting critical temperature, T_c , of 203 K near 150 GPa was reported for H_3S ⁶, followed by a T_c of 260 K near 200 GPa in LaH_{10} ^{7;8}. Recently, a carbonaceous sulfur hydride superconductor with a measured T_c of 288 K at 267 GPa was discovered⁹, but many questions remain unanswered about this material. Perhaps the most pressing of these questions is: “What is the composition and structure of the phase, or phases, responsible for the remarkably high T_c ?” Recent x-ray diffraction (XRD) studies suggest the material is derived from the Al_2Cu structure type up to 180 GPa^{10;11}, but its evolution upon further compression where the T_c is highest has not yet been determined experimentally. The reported T_c versus pressure⁹ shows evidence for a transition near 200 GPa, although the scatter in the data are consistent with a continuous change in T_c . On the other hand, the XRD results suggest that this change in T_c could arise from the collapse of the observed lower symmetry orthorhombic to higher symmetry superconducting phases.¹¹

To understand the nature of carbonaceous sulfur hydride, it is useful to review the work leading to the discovery of the initial high- T_c H_3S superconductor¹². Synthesis of novel $(\text{H}_2\text{S})_2\text{H}_2$ van der Waals compounds at pressures up to 40 GPa¹³ inspired the computational search for additional H-S phases that might be stable and potentially superconducting at megabar pressures.^{14;15} An $Im\bar{3}m$ symmetry H_3S phase, which can be described as a body centered cubic sulfur lattice with H atoms lying midway between adjacent S atoms ($T_c=191\text{-}204$ K at 200 GPa), was predicted to be stable above 180 GPa. An analogous lower-symmetry $R\bar{3}m$ phase with asymmetric H-S bonds was preferred at pressures down to 110 GPa ($T_c=155\text{-}166$ K at 130 GPa)¹⁵. Experiments on the H-S system confirmed the maximum T_c (203 K) near the expected pressures (155 GPa), leading to the proposal that the synthesized structure was the predicted $Im\bar{3}m$ phase⁶. Subsequently XRD measurements largely confirmed the predicted cubic structure^{16;17}. However, the synthesis conditions were found to dictate the product that formed, and T_c s as low as 33 K were measured. Thus, reproducing the synthesis of the cubic phase proved difficult^{18;19}, and more recently altogether new structures have been reported²⁰.

These observations suggest that a number of H_xS_y superconductors can be made. Indeed, additional peaks observed in XRD measurements have been assigned to possible secondary phases^{16;19}. Various stoichiometries including H_2S ^{14;21}, HS_2 ²², H_4S_3 ²³, and H_5S_2 ²⁴ have been proposed for materials with lower T_c s. Exotic Magnéli phases with H_xS_{1-x} ($2/3 < x < 3/4$) compositions characterized by alternating H_2S and H_3S regions with a long modulation whose ratio can be varied to tune the T_c have also been proposed²⁵. First-principles calculations suggested that H_2S self-ionizes under pressure forming a $(\text{SH}^-)(\text{H}_3\text{S}^+)$ perovskite-type structure²⁶ that may undergo further deformations to a complex modulated phase^{27;28}. A $Z = 24$ $R\bar{3}m$ symmetry phase whose density of states (DOS) at the Fermi level (E_F) was predicted to be lower than that of $R\bar{3}m$ and $Im\bar{3}m$ H_3S was computed to be more stable than these two phases between 110-165 GPa²⁹. The role

of quantum nuclear and anharmonic effects on the $R3m \rightarrow Im\bar{3}m$ transition and T_c has been investigated^{30;31}, as has the response of the Fermi surface to uniaxial strain³².

Turning to the C-S-H ternary, initial crystal structure prediction calculations conducted prior to the discovery of the carbonaceous sulfur hydride superconductor considered stoichiometric $C_xS_yH_z$ compositions with relatively high carbon dopings^{33;34}. These studies identified metastable CSH₇ structures that were based on the intercalation of methane into an H₃S framework, with maximum T_c s estimated to be 194 K at 150 GPa³³ and 181 K at 100 GPa³⁴. However, the measured structural parameters, P - V equations of state¹¹, and the variation of T_c versus pressure⁹ do not match those calculated for these hydride perovskite-like materials. First-principles calculations employing the virtual crystal approximation (VCA) predicted that remarkably low-level hole-doping resulting from the incorporation of carbon in the parent H₃S phase (i.e. C_{0.038}S_{0.962}H₃) could increase the T_c up to 288 K^{35;36}. It was argued that doping tunes the position of E_F , moving it closer to the maximum in the DOS that arises from the presence of two van Hove singularities (vHs). Because vHs increase the number of states that can participate in the electron-phonon-coupling (EPC) mechanism, this effect is known in general to enhance the total coupling strength, λ , and in turn the T_c in conventional superconductors. The role that the vHs play in increasing the T_c in H₃S has been studied in detail³⁷⁻⁴⁰.

Despite the striking success of the VCA model in reproducing theoretically the very high T_c measured for the C-S-H superconductor³⁵, this approach does not take into account the effect of the doping on the local structure and electronic properties, and its limitations have been discussed^{41;42}. To overcome these limitations we systematically study the role of doping on the thermodynamic and dynamic stability, electronic structure, and geometric properties of phases with doping levels as low as 1.85%. Three types of substitutions are considered involving S replaced by C, together with different numbers of hydrogens, yielding either six-fold or four-fold coordinate carbon atoms. We find that CH₆ and CH₄ form stable configurations within the dense solid in phases that are dynamically stable at the pressures studied experimentally. Moreover, doping *decreases* the DOS at E_F because it breaks degeneracies and localizes electrons in C-H bonds. Our results illustrate that the rigid band model does not reliably predict the superconducting properties of the doped phases. Finally, the descriptors associated with superconductivity, such as the DOS at E_F and the logarithmic average phonon frequency are used to identify the C-S-H phase likely to possess the highest T_c .

Results and Discussion

Octahedrally Coordinated Carbon in C_xS_{1-x}H₃ Phases

To investigate how different levels of doping affect the kinetic and thermodynamic stability, electronic structure, and superconducting properties of H₃S, we constructed supercells of the $Im\bar{3}m$ structure where one of the sulfur atoms was replaced by carbon. Calculations were carried out at 270 GPa with C_xS_{1-x}H₃ stoichiometries and two different types of coordination environments around the dopant atom were considered. In the first the carbon atom was octahedrally coordinated by six hydrogen atoms, and in the second two of these

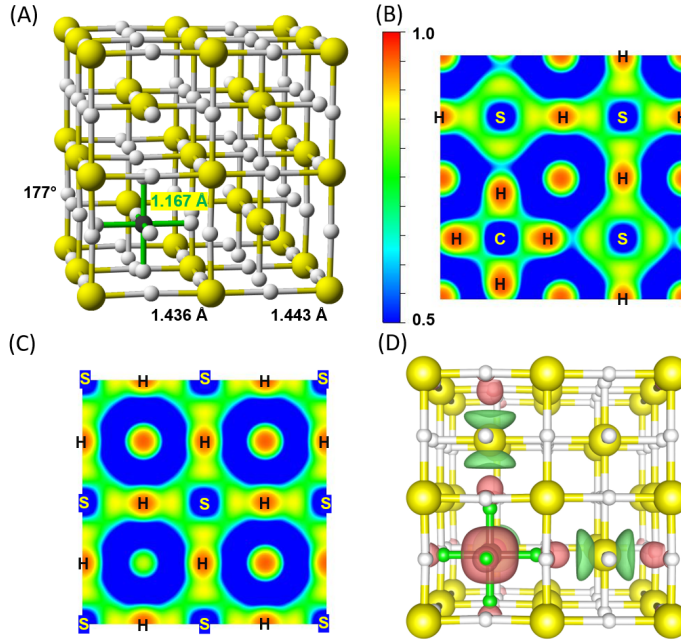


Figure 1: (a) Optimized geometry and (b,c) electron localization function (ELF) contour plot of $C_{0.0625}S_{0.9375}H_3$ (O_h - $CS_{15}H_{48}$, space group $Pm\bar{3}m$), where the carbon atom is octahedrally coordinated by hydrogen atoms at 270 GPa. The plane of the contour passes through (b) CH_6 and (c) H_3S , and the range of the isovalues is from 0.5 (blue/cold) to 1.0 (red/warm). The atoms through which the plane passes are labelled. (d) The following electron density difference: $\rho(CH_6) + \rho(S_{15}H_{48}) - \rho(CS_{15}H_{48})$ where red denotes a loss of charge and green a gain of charge (isovalue=0.005). Sulfur/carbon/hydrogen atoms are yellow/black/white and select geometric parameters are provided.

C-H bonds broke resulting in a quasi-tetrahedral CH_4 molecule. A detailed analysis was carried out on the $C_{0.0625}S_{0.9375}H_3$ ($CS_{15}H_{48}$) stoichiometry at 270 GPa because both geometries were dynamically stable at this pressure (Figure S2d, S10c), and because this unit cell size pushes the limits of the phonon and EPC calculations.

The calculated C-H distance in the octahedrally coordinated phase, which we refer to as O_h - $CS_{15}H_{48}$ (Figure 1a), measures 1.17 Å. The negative of the crystal orbital Hamilton population integrated to the Fermi level (-iCOHP), which can be used to quantify the bond strength, is calculated to be 5.11 eV for this bond. The distance between the hydrogen atom bonded to carbon and its nearest neighbor sulfur (1.71 Å), is significantly larger than the H-S distance found in $Im\bar{3}m$ H_3S at this pressure (1.45 Å). The weakening of the CH-S bond upon doping is evident in the -iCOHP, which decreases from 3.74 eV/bond (in H_3S) to 2.00 eV/bond. Despite the non-negligible -iCOHPs between the hydrogen atoms bonded to carbon and the nearest neighbor sulfur atoms, the ELF (Figure 1b,c) does not show any evidence of covalent CH-S bond formation. The integrated crystal orbital bond index

(iCOBI), which is a quantification of the extent of covalent bond formation⁴³, is calculated to be 0.34 for each S-H bond in H₃S, indicating a bond order of roughly 1/3. Substituting C in an octahedral coordination environment leaves the S-H iCOBI essentially unchanged for bonds distant from the C substitution site, but for CH-S bonds the iCOBI drops to 0.21, showing the weakening of this bond. Practically no antibonding states are filled in the S-H interaction with H coordinating C (Figure S6), but the increased S-H distance leads to an overall decrease in the magnitude of the iCOBI. The C-H bonds in the octahedral CH₆ motif possess the largest iCOBI in the system, 0.51. Subtracting the charge density of the CS₁₅H₄₈ structure from a sum of the density arising from the neutral CH₆ molecule and the neutral H-S framework (Figure 1d) illustrates that charge is transferred from the CH₆ unit into the nearest neighbor sulfur lone pairs, which can also be seen in the ELF plot (Figure 1b). A Bader analysis, which typically underestimates the formal charge, yields a +0.25 charge on CH₆, indicating that charge redistribution is associated with stabilization of this configuration in the dense structure.

An analysis using the reversed approximation Molecular Orbital (raMO) method, which uses linear combinations of the occupied crystal orbitals of the system to reproduce target orbitals, revealed substantial bonding interactions within the CH₆ cluster. The reproduced *s* orbital on the hydrogen atom in this motif contained electron density with *p*-orbital symmetry on the neighboring C atom, indicative of *sp* bonding. Similarly, the reproduced *s* orbital on C strongly interacted with the surrounding H atoms, which is evident in its anisotropy as comparison to the more isotropic sulfur *s* orbital reproductions (Figure S7).

Theoretical considerations have been key in designing ways to stabilize four-coordinate carbon in novel bonding configurations such as planar tetracoordinate carbon^{44;45}. While a wide variety of molecular compounds containing coordination numbers surpassing four, such as carbocations, carboranes, organometallics, and carbon clusters, are also known^{46;47}, octahedrally coordinated carbon is quite unusual. Examples include elemental carbon, which has been predicted to become six-fold coordination at terapascal pressures^{48;49}, and high pressure Si-C compounds such as rock-salt SiC^{50;51}, and two predicted Si₃C phases⁵². More relevant to the C-S-H system are carbon atoms bonded to more than four hydrogen atoms such as the nonclassical carbocation, C_s-CH₅⁺, which contains three short and two long C-H bonds. It can be viewed as a proton inserted into one of the σ C-H bonds within methane, forming a three-center two-electron (3c-2e) bond between one carbon and two hydrogen atoms⁵³. *Ab initio* calculations for the isolated molecule have shown that the minimum energy configuration for the di-carbocation, CH₆²⁺, possesses C_{2v} symmetry with two long 3c-2e and two short classic 2c-2e bonds, rather than the O_h symmetry CH₆²⁺ geometry^{54;55}. Following one of the triply degenerate imaginary normal modes, which can be described as a wagging motion along the three sets of H-C-H 180° angles in the octahedron, leads to the C_{2v} minimum. Turning now to hypercoordinated carbon atom in the O_h-CS₁₅H₄₈ model structure, explicit calculation of the phonons at the Γ point reveals that in the solid state the frequency of this same triply degenerate mode is real (calculated frequency of 1712 cm⁻¹), and the vibration is coupled with the motions of the hydrogens in the H₃S lattice. Thus, the stabilization of the octahedral molecular complex is facilitated by weak interactions with the host lattice. Notably, the calculated C-H bond length in CH₆²⁺ obtained at the HF/6-311+G(2d,p) level of theory, is nearly identical to that of

O_h -CS₁₅H₄₈ at 270 GPa (both ~ 1.17 Å). That the carbon weakly interacts with the host lattice is supported by calculations where the carbon (or sulfur) is replaced with neon. The optimized O_h -NeS₁₅H₄₈ structure is dynamically stable at these pressures, with a calculated Ne-H distance of 1.37 Å (Figure S30).

Quasi-Tetrahedrally Coordinated Carbon in $C_xS_{1-x}H_3$ Phases

When placed in a cube a tetrahedral methane molecule can retain its symmetry only if its hydrogens point toward four corners of the cube. In the phases studied here such an orientation introduces unfavorable steric interactions, and a lower enthalpy can be obtained when the hydrogens point towards four cube faces instead. Because of this the four coordinate CH₄ species within the phase we refer to as T_d -CS₁₅H₄₈ actually possesses C_{2v} symmetry. As illustrated in Figure 2a, at 270 GPa its two C-H bond lengths are nearly identical with calculated ρ -COHPs of 6.34 and 6.30 eV/bond. The H-S distances between two of the hydrogens bonded to carbon elongate to 1.73 Å, and a further two to 1.91 Å. At the same time two of the S-H bonds contract relative to those within $Im\bar{3}m$ H₃S (1.34 Å). The encapsulated methane molecule possesses H-C-H angles that deviate from the ideal tetrahedral angle (100°, 103° and 140°), and its Bader charge, -0.09, is suggestive of electron donation from the H-S lattice. Plots of the ELF (Figure 2b) clearly illustrate the C-H bond, but do not show any evidence of covalent bond formation between CH₄ and the H-S framework. Thus, two H-S and four C-H bonds per unit cell in T_d -CS₁₅H₄₈ become classical 2c-2e bonds, no longer participating in delocalized multi-centered bonding as they would within H₃S.

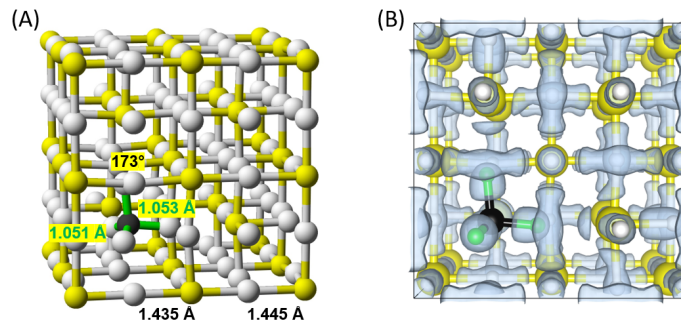


Figure 2: (a) Optimized geometry and (b) electron localization function (ELF; iso-value=0.8) of the CH₄-based C_{0.0625}S_{0.9375}H₃ (T_d -CS₁₅H₄₈, space group $Am\bar{m}2$) in which the carbon atom is quasi-tetrahedrally coordinated by hydrogen atoms at 270 GPa. Sulfur/carbon/hydrogen atoms are yellow/black/white and select geometric parameters are provided.

Properties of the S \rightarrow C Doped Phases at 270 GPa

Our calculations find the DOS at the Fermi level, N_F , in H_3S to be 0.050 states $\text{eV}^{-1}\text{\AA}^{-3}$ at 270 GPa. Moving E_F down in energy by 0.17 eV, which can be achieved by doping with $\sim 5.7\%$ C, yields the highest possible value of 0.055 states $\text{eV}^{-1}\text{\AA}^{-3}$. Given a reference material whose superconducting critical temperature, T_c^0 , is known, the approximate Bardeen-Cooper-Schrieffer formula can be employed to estimate the T_c of a similar material via the formula $T_c = 1.13\Theta_D(T_c^0/1.13\Theta_D^0)^{N_F^0/N_F}$, where Θ_D is the Debye temperature and N_F is given per unit volume⁵⁶. Using the measured value of $T_c^0 = 170$ K at 270 GPa for $Im\bar{3}m$ H_3S ¹⁷, this simple model predicts the T_c to increase to 208 K for $\sim 5.7\%$ C doping, which is somewhat lower than the results obtained using the VCA at the same pressure and doping level³⁵.

To study the effect of doping on the electronic structure, we performed a single point calculation on an unrelaxed $2 \times 2 \times 2$ supercell of $Im\bar{3}m$ H_3S where a single sulfur atom was replaced by carbon. In contrast to the VCA model predictions we found that N_F decreases to 0.048 states $\text{eV}^{-1}\text{\AA}^{-3}$. Structural relaxation to the O_h - and T_d - $\text{CS}_{15}\text{H}_{48}$ phases further lowers N_F to 0.040 and 0.033 states $\text{eV}^{-1}\text{\AA}^{-3}$, respectively, as illustrated in Figure 3. This initially counter-intuitive behavior of N_F can be understood by considering the following: replacing sulfur by carbon followed by structural relaxation decreases the number of degenerate bands near E_F because some of the metallic electrons that were delocalized in the H_3S framework now become localized in covalent C-H bonds. Whereas 14 bands (some of which are degenerate) cross $E_F - 0.17$ eV in $Im\bar{3}m$ H_3S at 270 GPa, only 11 bands intersect with the Fermi level within both O_h - and T_d - $\text{CS}_{15}\text{H}_{48}$ (Figure 3a-3c).

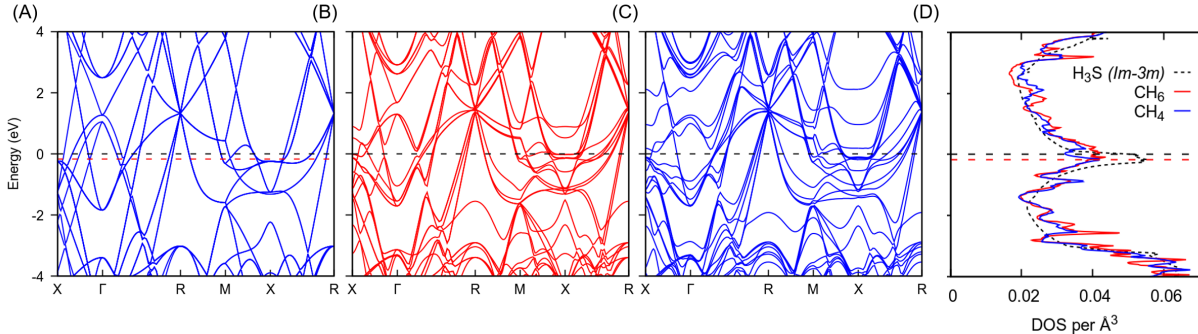


Figure 3: Band structure at 270 GPa for (a) $Im\bar{3}m$ H_3S in a $2 \times 2 \times 2$ supercell of the standard conventional lattice, (b) $Pm\bar{3}m$ O_h - $\text{CS}_{15}\text{H}_{48}$, and (c) $Amm2$ T_d - $\text{CS}_{15}\text{H}_{48}$. To compare the band structures of the three phases, which all possess different space-groups, simple cubic symmetry is assumed and the high symmetry special points used are Γ (0,0,0), X (0.5,0,0), M (0.5,0.5,0) and R (0.5,0.5,0.5). (d) Densities of states of these phases where CH_6 denotes $\text{CS}_{15}\text{H}_{48}$ with hexacoordinate carbon and CH_4 with tetracoordinate carbon. The black horizontal dashed line denotes E_F and the red dashed line $E_F - 0.17$ eV, which corresponds to the top of the peak in the DOS in $Im\bar{3}m$ H_3S .

We also investigated how the vibrational properties of $Im\bar{3}m$ H_3S are affected by carbon doping. The Debye temperature of the phase in which carbon is four-coordinate is larger than that containing six-coordinated carbon, which is higher than that of pure H_3S (Figure S24). The frequencies of the asymmetric H-C-H stretching modes of T_d - $CS_{15}H_{48}$ were calculated to be 3125 and 3286 cm^{-1} , whereas the symmetric ones occurred at 3140 and 3173 cm^{-1} . O_h - $CS_{15}H_{48}$ possessed a single C-H stretching mode at 2358 cm^{-1} . Because the quasi-molecular CH_4 species has stronger and shorter C-H bonds as compared to the octahedrally coordinated carbon, these vibrations are found at higher frequencies.

$C_xS_{1-x}H_3$ Phases as a Function of Doping and Pressure

We now consider the dynamic stability of the $C_xS_{1-x}H_3$ stoichiometries as a function of doping at 270 GPa, beginning with phases where carbon is octahedrally coordinated. Both the H-S and H-C bond lengths in the 50% doped dynamically unstable CSH_6 structure measured 1.37 Å. A majority of the phonon modes that were imaginary at some point within the Brillouin Zone (BZ) turned out to be related to the motions of the hydrogen atoms bonded to carbon. Decreasing the doping level to 25% allowed the C-H and S-H bonds to assume different values (1.08 Å and 1.41-1.44 Å, respectively). As a result, some of the imaginary modes in the 50% doped structure become real, specifically the asymmetric and symmetric H-C-H stretching modes found near ~ 2700 and 2500 cm^{-1} , respectively. Lowering the doping level left a single imaginary phonon mode throughout the whole BZ. This mode arose from the movement of a hydrogen atom sandwiched between two carbons that led to the lengthening of one, and contraction of another C-H bond that measured 1.43 Å in the optimized geometry. The other C-H bond in this structure measured 1.13 Å. Thus, the structural instability is a result of the too-long C-H bonds that arise because of the constraints imposed by the doping level and S-H lattice.

The O_h - $CS_{15}H_{48}$ phase possesses the stoichiometry with the lowest percentage doping that is a local minimum at 270 GPa. Phonon calculations showed this structure becomes dynamically unstable below 255 GPa (Figure S4). Visualization of one of the triply degenerate imaginary modes at Γ revealed that it can be described as a lengthening/contraction of the CH-S distance, which measured 1.73 Å in the optimized structure, with the other two modes corresponding to the same vibration but along the other crystallographic axes. Upon decreasing pressure from 270 to 240 GPa the C-H bond length increased minimally ($\Delta d = 0.005$ Å, $-\Delta iCOHP = 0.02$ eV/bond), whereas the increase in the CH-S distance was an order of magnitude larger ($\Delta d = 0.03$ Å, $-\Delta iCOHP = 0.10$ eV/bond). These results suggest that the instability that emerges near 255 GPa is primarily a result of decreased S-H interaction at lower pressures.

We also consider O_h - $CS_{53}H_{162}$, which corresponds to 1.85% doping, with calculated C-H bond lengths of 1.16 Å and S-H bonds ranging from 1.43-1.48 Å. Unsurprisingly, its DOS at E_F of 0.0484 states $eV^{-1}\text{Å}^{-3}$ and Debye temperature of 1375 K approach the values obtained for $Im\bar{3}m$ H_3S . Phonon calculations revealed that this phase was dynamically stable at 270 GPa, and it could be stabilized to lower pressures than O_h - $CS_{15}H_{48}$, becoming unstable at approximately 160 GPa. The structures that possess four-coordinated carbon atoms are found to be dynamically stable at 270 GPa when the doping level was less

than 25% (CS_3H_{12} , CS_7H_{24} , $\text{CS}_{15}\text{H}_{48}$ and $\text{CS}_{53}\text{H}_{162}$). CS_3H_{12} was unstable by 140 GPa and visualization of the largest magnitude imaginary mode found at the R point illustrated that it corresponded to a symmetric/asymmetric H-S-H stretch. CS_7H_{24} and $\text{CS}_{15}\text{H}_{48}$ became dynamically unstable near 250 GPa via a softening of the longitudinal acoustic mode at an off Γ point, and $T_d\text{-CS}_{53}\text{H}_{162}$ was stable (unstable) at 200 (160) GPa.

$\text{C}_x\text{S}_{1-x}\text{H}_{3+x}$ Phases: Doping H_3S via Substituting SH_3 by CH_4

Instead of replacing a fraction of the S atoms by C atoms, another way to dope H_3S would be to replace some of the SH_3 units by CH_4 in a large supercell. Indeed, XRD and equation of state analysis show that the precursor phases of the C-S-H superconductor are $(\text{H}_2\text{S})_2\text{H}_2$ and $(\text{CH}_4)_2\text{H}_2$ van der Waals compounds that have identical volumes at the synthesis pressure, thereby allowing readily mixed $(\text{H}_2\text{S}, \text{CH}_4)_2\text{H}_2$ alloys¹¹. This leads to the possibility that CH_4 molecules persist in the structure well into the superconducting H_3S -based phase or phases with H_2 taken up in the structure. First-principles calculations have previously been employed to investigate the properties of metastable phases that correspond to 50% $\text{SH}_3 \rightarrow \text{CH}_4$ substitution, wherein methane molecules were intercalated in an H_3S framework.^{33;34} Lower dopings could be derived from the $T_d\text{-C}_x\text{S}_{1-x}\text{H}_3$ phases discussed above by adding a single hydrogen atom to the S-H lattice. Unlike structures in which C replaced S, all of the CH_4 dopings we considered (25, 12.5, 6.25 and 1.85% C) were found to be dynamically stable at 270 GPa and remained so on decompression to at least 140 GPa (Figures S17, S19-S22).

The optimized geometry obtained by taking a sixteen formula unit supercell and replacing one SH_3 by CH_4 , corresponding to a stoichiometry of $\text{CS}_{15}\text{H}_{49}$, is illustrated in Figure S16c³³. The Bader charge on the C_{3v} symmetry methane molecule was nearly the same as in $T_d\text{-CS}_{15}\text{H}_{48}$, -0.10 , but the bonds were somewhat shorter and stronger (1.03 Å and 6.92 eV/bond ($\times 1$), 1.04 Å and 6.98 eV/bond ($\times 3$)) and the angles were closer to those of a perfect tetrahedron (105° , 113°). The DOS at E_F of $\text{CS}_{15}\text{H}_{49}$ (0.034 states $\text{eV}^{-1}\text{Å}^{-3}$) is quite comparable to that of $T_d\text{-CS}_{15}\text{H}_{48}$, but its Debye temperature is significantly higher (1825 K, Figure S24), suggesting that its T_c may be higher as well.

Thermodynamic Properties and Equation of States

The relative enthalpies of the doped structures from H_3S , as well as carbon in the diamond phase and the $C2/c$ phase of molecular H_2 (Figure 4) illustrate that doping is thermodynamically unfavorable within the pressure range considered, consistent with previous studies of carbon doped SH_3 phases^{33;34;36;41}. For a given number of C+S atoms the phase where CH_4 replaced H_3S was always the most stable, followed by phases where a tetrahedrally coordinated C replaced an S atom, and lastly those where C was octahedrally coordinated. Exploratory calculations suggested that it was not enthalpically favorable to add another hydrogen to the $\text{SH}_3 \rightarrow \text{CH}_4$ doped phases by forming another S-H bond (e.g. ΔH for the reaction $\text{CS}_3\text{H}_{13} + \frac{1}{2}\text{H}_2 \rightarrow \text{CS}_3\text{H}_{14}$ was +17.8 meV/atom).

The enthalpies of the phases with the lowest levels of doping were within < 2 meV/atom of each other, and they were the closest to the threshold for thermodynamic stability, with

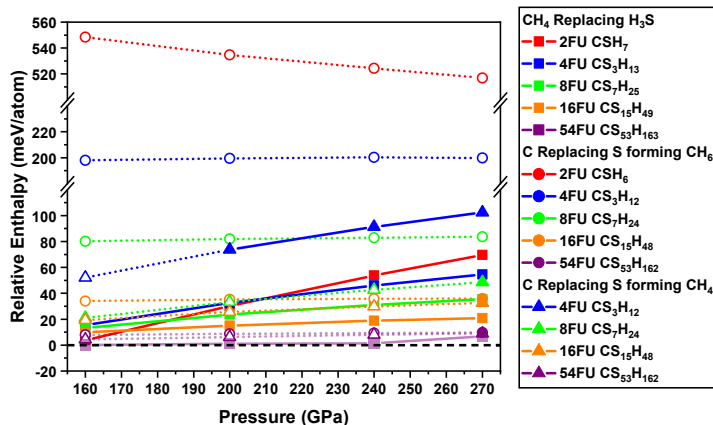


Figure 4: ΔH as a function of pressure for the following reaction: $C + x(\text{H}_3\text{S}) + \left(\frac{y-3x}{2}\right) \text{H}_2 \rightarrow \text{CS}_x\text{H}_y$ in meV/atom using the diamond phase of carbon⁵⁷, $C2/c$ phase of H_2 ⁵⁸ and $Im\bar{3}m$ phase of H_3S ¹⁴ as a reference. The open (closed) circles correspond to structures that were found to be dynamically unstable (stable).

ΔH for the formation of $\text{CS}_{53}\text{H}_{163}$ being 0.14 and 6.82 meV/atom at 140 and 270 GPa, respectively. At 270 GPa the zero-point-energy disfavored the doped species where carbon was tetrahedrally coordinated (Table S2) but this had less of an effect on the octahedrally coordinated systems, such that for $\text{S} \rightarrow \text{C}$ replacements, the structures in which C was six coordinate became slightly preferred. Even though the carbon doped phases are not thermodynamically stable, their enthalpies of formation are generally within the ~ 70 meV/atom threshold corresponding to the 90th percentile of DFT-calculated metastability for inorganic crystalline materials at 1 atm⁵⁹.

Superconducting Properties

In addition to the phonon band structures and phonon densities of states, we calculated the Eliashberg spectral function, $\alpha^2 F(\omega)$, and the EPC integral, $\lambda(\omega)$, for the model structures considered here (Figure S1d, S7a, and S16a). Initially, $O_h\text{-CS}_{15}\text{H}_{48}$ was singled out for analysis because its high N_F relative to other carbon-doped phases suggests it may have the highest T_c . Calculations for structures with lower carbon concentrations are currently computationally unfeasible because of their large supercells. Since T_c is usually highest near the onset of dynamic instability the calculation was performed at 255 GPa (Figure S27). The estimated EPC (Table 1) was a modest $\lambda = 1.09$, with 27% arising from the low frequency modes associated with the motions of the sulfur atoms ($< 700 \text{ cm}^{-1}$), and 72.5% resulting from motions predominantly due to the hydrogen atoms bonded to sulfur, with a minor contribution from the hydrogens bonded to carbon ($700\text{-}2200 \text{ cm}^{-1}$). Numerical solution of the Eliashberg equations using a typical value of the Coulomb pseudopotential, $\mu^* = 0.1$, resulted in a T_c of 136 K at 255 GPa.

The T_c computed for $O_h\text{-CS}_{15}\text{H}_{48}$ is over 100 K lower than the maximum measured for

Table 1: Debye temperature (Θ_D), density of states at the Fermi level (N_F , in states/eV/ \AA^3), logarithmic average of phonon frequencies (ω_{ln}), electron-phonon coupling constant (λ), and superconducting critical temperature (T_c) obtained via numerical solution of the Eliashberg equations using $\mu^* = 0.1$ at 270 GPa. The pressure range where dynamic stability was confirmed in this study (phonon calculations were carried out between 140-270 GPa) is also provided.

Structure	Θ_D (K)	N_F	ω_{ln} (K)	λ	T_c (K)	P_{stab} (GPa)
$Im\bar{3}m$ H ₃ S	1314	0.0502	1603	1.25	174	N/A
$R\bar{3}m$ H ₃ S	1340	0.0440	1615	0.95	140	N/A
^a O_h -CS ₁₅ H ₄₈	1449	0.0401				260-270
O_h -CS ₅₃ H ₁₆₂	1375	0.0484				200-270
T_d -CS ₃ H ₁₂	1813	0.0281	1370	0.85	80	180-270
T_d -CS ₇ H ₂₄	1875	0.0395				270
T_d -CS ₁₅ H ₄₈	1639	0.0325				270
T_d -CS ₅₃ H ₁₆₂	1774	0.0460				260-270
$Cmcm$ CSH ₇	1781	0.0256				140-270
$R\bar{3}m$ CSH ₇	1851	0.0275				140-270
CS ₃ H ₁₃	1821	0.0245	1704	1.01	142	140-270
CS ₇ H ₂₅	1868	0.0313				140-270
CS ₁₅ H ₄₉	1825	0.0343				140-270
^b CS ₅₃ H ₁₆₃	1818	0.0434				140-270

^a The computed values for this phase at 255 GPa are: $\Theta_D = 1490$ K, $N_F = 1414$ K, $\lambda = 1.09$, $T_c = 136$ K (numerically solving Eliashberg equations).

^b Assuming $\omega_{\text{ln}} = 1704$ K and $\lambda = 2.5$ yields $T_c = 280$ K (calculated using the Allen-Dynes modified McMillan equation – see text).

the C-S-H superconductor⁹, in agreement with recent results of Guan *et al.*⁴². Even though the Debye temperature of this phase is predicted to be higher than that of $Im\bar{3}m$ H₃S (at 270 GPa), its ω_{ln} is lower, as is the λ and resulting T_c predicted by the present approach. Decreasing the doping level will increase T_c . Nonetheless, our results suggest that the superconducting properties of structures belonging to this family are unlikely to surpass those of $Im\bar{3}m$ H₃S because N_F of the doped phase is lower, but the Debye temperatures are similar (cf. values obtained at 270 GPa in Table 1).

We now examine whether tetrahedral coordination of the carbon atoms can enhance T_c . Unfortunately, because the symmetries of T_d -CS₁₅H₄₈ and CS₁₅H₄₉ are lower than that of O_h -CS₁₅H₄₈ calculating their T_c s was prohibitively expensive. Therefore, 25% doped systems were considered instead. Despite the fact that the estimated Debye temperature for T_d -CS₁₅H₄₈ was higher than that of H₃S, ω_{ln} was lower, mirroring the findings for O_h -CS₁₅H₄₈. In addition, the EPC was lower, consistent with the much smaller N_F , resulting in a T_c of 80 K. Even though decreasing the doping increases N_F , once again it is unlikely that compounds belonging to this family of structures could be superconducting at temperatures higher than those found for H₃S. However, adding one more hydrogen atom per unit cell to members of this family leads to a remarkable improvement. Both ω_{ln} and λ of CS₃H₁₃

are higher than that of T_d -CS₃H₁₂, yielding a T_c of 142 K at 270 GPa. Thus, a little bit of carbon does a lot for superconductivity in H₃S, and the way in which it is altered (whether it be an increase or decrease) is intimately related to the local bonding configuration around carbon.

To better understand how adding a single hydrogen atom can dramatically increase T_c by 60 K, we compare $\lambda(\omega)$ and $\omega_{\text{ln}}(\omega)$ of these two model structures (Figure S24). At $\sim 1550 \text{ cm}^{-1}$ their $\omega_{\text{ln}}(\omega)$ are almost identical. At higher frequencies $\omega_{\text{ln}}(\omega)$ for CS₃H₁₃ increases much faster until a near plateau region is attained at 2220 cm^{-1} (1670 K). In T_d -CS₃H₁₂, on the other hand, $\omega_{\text{ln}}(\omega)$ reaches 1309 K at 2450 cm^{-1} . Beyond $\sim 2500 \text{ cm}^{-1}$, the flat high-frequency bands contribute less than 40 K to $\omega_{\text{ln}}(\omega)$ for both structures. Therefore, the main difference in the total ω_{ln} for the two phases arises from modes in the 1550-2500 cm^{-1} frequency range. From the projected phonon density of states (Figure S10a and S17a) modes associated with motions of the H atoms in the H-S lattice (H1) primarily comprise this region, with some contribution from H atoms in the CH₄ molecule (H2). At $\sim 1410 \text{ cm}^{-1}$ $\lambda(\omega)$ was almost the same for the two structures (~ 0.45). At higher frequencies the $\lambda(\omega)$ for CS₃H₁₃ increases much faster until 2220 cm^{-1} where it reaches a value of 1.00, while for T_d -CS₃H₁₂ $\lambda(\omega)$ reaches 0.83 at 2450 cm^{-1} . Beyond $\sim 2500 \text{ cm}^{-1}$, the high-frequency flat bands contribute less than 0.005 towards λ for both structures.

Additional insight into the types of motions that result in a larger λ within CS₃H₁₃ can be obtained by visualizing selected vibrational modes that have a notable $\lambda_{\mathbf{q}\nu}$, e.g., modes about halfway along the Y \rightarrow Z (1412 cm^{-1}) and Z \rightarrow L (1361 cm^{-1}) paths, which have very large contributions (Figure 5). Both of these involve H2 vibrations between neighboring S atoms, leading to a snakelike undulation of the H1/H2 chains. The addition of the extra S-bonded H atom expands the S-H lattice in the ab plane, leaving looser contacts between the S and H atoms (1.44 \AA and 1.43 \AA as opposed to 1.41 - 1.43 \AA in T_d -CS₃H₁₂), thereby softening the phonon frequencies. The c axis is largely unchanged by the addition of an extra H, but the H-S distances that are relatively even in CS₃H₁₂ (1.43 - 1.44 \AA) become disproportionate in CS₃H₁₃ to 1.41 and 1.46 \AA . Within the methane fragments, two H1 atoms possessed mirrored circular motions that were part of the undulating H chains.

Although decreasing the doping does not appreciably change the Debye temperature, it increases the N_F substantially such that at 1.85% doping the value is almost double that of the 25% doped phase. Assuming that ω_{ln} for CS₅₃H₁₆₃ is close to that for CS₃H₁₃ a T_c of 280 K could be obtained using the Allen-Dynes modified McMillan equation⁶⁰ for $\lambda \sim 2.5$. Since this approximate equation is known to underestimate T_c s for systems where $\lambda \geq 1.5$, within the Eliashberg formalism somewhat smaller λ values would yield a similar result. Therefore, it is plausible that the λ of CS₅₃H₁₆₃ could fall within this range given its high N_F . For comparison, at 200 GPa $Im\bar{3}m$ H₃S is computed to have a similar λ (2.19), but its ω_{ln} (1335 K) is significantly smaller, yielding an estimated T_c of 191-204 K¹⁵. Moreover, its DOS at E_F , $0.041 \text{ states/eV/\AA}^3$, is comparable to that obtained for CS₅₃H₁₆₃. It is beyond the scope of this study to explicitly calculate the T_c of C _{x} S _{$1-x$} H _{$3+x$} phases over a broad range of doping levels (e.g., 1.85-12.5%). We note that unlike the other families of structures studied to date, structures belonging to this family were found to be dynamically stable across a broad pressure range (at least 140-270 GPa).

In summary, our detailed computations have shown that doping H₃S by 1.85-25% of

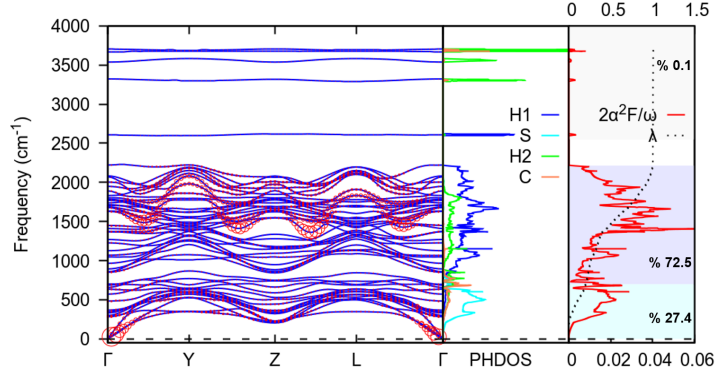


Figure 5: Phonon band structure, phonon density of states (PHDOS), Eliashberg spectral function in the form of $\frac{2\alpha^2 F(\omega)}{\omega}$, and the electron phonon integral, $\lambda(\omega)$, for CS_3H_{13} at 270 GPa. Red circles indicate the electron-phonon coupling constant, $\lambda_{q\nu}$, at mode ν and wavevector q , and their radii is proportional to the strength. H1 are the hydrogen atoms in the S-H lattice, and H2 are the hydrogen atoms in CH_4 . The percentages given were calculated via $\left(\int_{\omega_1}^{\omega_2} \lambda(\omega) d\omega / \lambda\right) \times 100\%$; and the frequency regions spanning ω_1 and ω_2 are colored coded in the PHDOS.

carbon at 270 GPa leads to a plethora of metastable phases where carbon can be either six-coordinated or four-coordinated to hydrogen. In the first case we see the remarkable emergence of an O_h symmetry CH_6 motif reminiscent of a di-carbocation, but stabilized in the solid state under pressure via weak interactions by the negatively charged environment of the surrounding host H_3S -like lattice. The second case is an example of methane intercalated within an H_3S -like framework. These doping schemes split degenerate bands thereby decreasing N_F , and localizing electrons in covalent C-H bonds whose signatures are far removed from the Fermi energy.

Both ω_{ln} and λ of $O_h\text{-CS}_{15}\text{H}_{48}$ and $T_d\text{-CS}_3\text{H}_{12}$ were smaller than the values computed for $Im\bar{3}m$ H_3S , as was the resulting T_c . Remarkably, adding a single hydrogen atom to $T_d\text{-CS}_3\text{H}_{12}$ increased T_c by 60 K. The larger λ and ω_{ln} of the resulting CS_3H_{13} phase could be traced back to the emergence of soft phonon modes, a consequence of the weaker and longer S-H bonds in the host lattice caused by the insertion of the extra S-bonded hydrogen atom. At 270 GPa the T_c of CS_3H_{13} was about the same as that of $R3m$ H_3S despite its much lower DOS at E_F . Decreasing the doping level in this family of structures, derived from H_3S by low-level incorporation of CH_4 , is likely to increase T_c further. We hope that the present results will stimulate further theoretical studies, large supercell calculations of the superconducting properties of these structures, as well as additional experiments in search of still higher T_c s and phases that may be stable over a broader range of conditions.

Methods

Electronic Structure Calculations

Geometry optimizations and electronic structure calculations were performed using density functional theory (DFT) with the Perdew-Burke-Ernzerhof (PBE) exchange correlation functional⁶¹ as implemented in the Vienna *Ab initio* Simulation Package (VASP) 5.4.1⁶². The valence electrons (H $1s^1$, S $3s^23p^4$, and C $2s^22p^2$) were treated explicitly using plane wave basis sets with a cutoff energy of 800 eV (as previously employed by Cui *et al.*³³), while the core states were treated with the projector-augmented wave (PAW)⁶³ method. The reciprocal space was sampled using a Γ -centered Monkhorst-Pack scheme, and the number of divisions along each reciprocal lattice vector was chosen such that the product of this number with the real lattice constant was 70 Å for the density of states (DOS) calculations, and 50 Å otherwise. The crystal orbital Hamilton populations (COHPs)⁶⁴, the negative of the COHPs integrated to the Fermi level (-iCOHPs), and the crystal orbital bond index (COBI)⁴³ were calculated using the LOBSTER package (v2.2.1 for -iCOHP and v4.1.0 for COBI)⁶⁵, and the results used to analyze the bonding. The dynamic stability of the phases was investigated via phonon calculations performed using the finite difference scheme as implemented in the PHONOPY software package⁶⁶. For the DFT-raMO procedure⁶⁷, single point calculations were carried out in VASP with coarse k -point grids sampling the full Brillouin zone with dimensions equal to the supercell used in the raMO analysis, corresponding to $3\times 3\times 3$ for $\text{CS}_{15}\text{H}_{48}$ and $5\times 5\times 5$ for H_3S .

Superconducting Properties

Phonon calculations were performed using the Quantum Espresso (QE)⁶⁸ package program to obtain the dynamical matrix and the electron-phonon coupling (EPC) parameters. The pseudopotentials were obtained from the PSLibrary⁶⁹ using H $1s^1$, S $3s^23p^4$, and C $2s^22p^2$ valence electrons and the PBE exchange-correlation functional⁶¹. Plane-wave basis set cutoff energies were set to 80 Ry for all systems. We employed a Γ -centered Monkhorst-Pack Brillouin zone sampling scheme, along with Methfessel-Paxton smearing with a broadening width of 0.02 Ry. Density functional perturbation theory (DFPT) as implemented in QE was employed for the phonon calculations. The EPC matrix elements were calculated using the k and q -meshes, and Gaussian broadenings listed in Table S1. The EPC parameter (λ) converges to within 0.05 for differences of the Gaussian broadening that are less than 0.02 Ry. The critical superconducting temperature, T_c , has been estimated using the Allen-Dynes modified McMillan equation⁶⁰, $T_c = \frac{\omega_{\text{ln}}}{1.2} \exp\left[-\frac{1.04(1+\lambda)}{\lambda-\mu^*(1+0.62\lambda)}\right]$, where ω_{ln} is the logarithmic average frequency, and μ^* was set to 0.1. The T_c were also obtained by solving the Eliashberg equations⁷⁰ numerically based on the spectral function, $\alpha^2F(\omega)$, obtained from the QE calculations.

References

- [1] Ashcroft, N. W. Hydrogen dominant metallic alloys: High temperature superconductors? *Phys. Rev. Lett.* **92**, 187002 (1–4) (2004)
- [2] Zurek, E., Hoffmann, R., Ashcroft, N. W., Oganov, A. R. & Lyakhov, A. O. A little bit of lithium does a lot for hydrogen. *Proc. Natl. Acad. Sci.* **106**, 17640–17643 (2009)
- [3] Zurek, E. & Bi, T. High-temperature superconductivity in alkaline and rare earth polyhydrides at high pressure: A theoretical perspective. *J. Chem. Phys.* **150**, 050901 (1–13) (2019)
- [4] Bi, T., Zarifi, N., Terpstra, T. & Zurek, E. in *The search for superconductivity in high pressure hydrides* (ed. Reedijk, J.) *Elsevier Reference Module in Chemistry, Molecular Sciences and Chemical Engineering* 1–36 (Elsevier, Waltham, MA, 2019)
- [5] Flores-Livas, J. A. *et al.* A perspective on conventional high-temperature superconductors at high pressure: Methods and materials. *Phys. Rep.* **856**, 1–78 (2020)
- [6] Drozdov, A. P., Eremets, M. I., Troyan, I. A., Ksenofontov, V. & Shylin, S. I. Conventional superconductivity at 203 kelvin at high pressures in the sulfur hydride system. *Nature* **525**, 73–76 (2015)
- [7] Somayazulu, M. *et al.* Evidence for superconductivity above 260 K in lanthanum superhydride at megabar pressures. *Phys. Rev. Lett.* **122**, 027001 (2019)
- [8] Drozdov, A. P. *et al.* Superconductivity at 250 K in lanthanum hydride under high pressures. *Nature* **569**, 528–531 (2019)
- [9] Snider, E. *et al.* Room-temperature superconductivity in a carbonaceous sulfur hydride. *Nature* **586**, 373–377 (2020)
- [10] Bykova, E. *et al.* Structure and composition of C-S-H compounds up to 143 GPa. *Phys. Rev. B* **103**, L14015 (2021)
- [11] Lamichhane, A. *et al.* X-ray diffraction and equation of state of the C-S-H room-temperature superconductor. *J. Chem. Phys.* **155**, 1 (2021)
- [12] Yao, Y. & Tse, J. S. Superconducting hydrogen sulfide. *Chem. Eur. J* **24**, 1769–1778 (2017)
- [13] Strobel, T. A., Ganesh, P., Somayazulu, M., Kent, P. R. C. & Hemley, R. J. Novel cooperative interactions and structural ordering in H₂S-H₂. *Phys. Rev. Lett.* **107**, 255503 (1–4) (2011)
- [14] Li, Y., Hao, J., Liu, H., Li, Y. & Ma, Y. The metallization and superconductivity of dense hydrogen sulfide. *J. Chem. Phys.* **140** (17), 174712 (1–7) (2014)

- [15] Duan, D. *et al.* Pressure-induced metallization of dense $(\text{H}_2\text{S})_2\text{H}_2$ with high- T_c superconductivity. *Sci. Rep.* **4**, 6968 (1–6) (2014)
- [16] Einaga, M. *et al.* Crystal structure of 200 K-superconducting phase of sulfur hydride system. *Nat. Phys.* **12**, 835–838 (2016)
- [17] Minkov, V. S., Prakapenka, V. B., Greenberg, E. & Erements, M. I. A boosted critical temperature of 166 K in superconducting D_3S synthesized from elemental sulfur and hydrogen. *Angew. Chem. Int. Ed.* **59**, 38970–18974 (2020)
- [18] Guigue, B., Marizy, A. & Loubeyre, P. Direct synthesis of pure H_3S from S and H elements: No evidence of the cubic superconducting phase up to 160 GPa. *Phys. Rev. B* **95** (2), 020104(R) (1–5) (2017)
- [19] Goncharov, A. F. *et al.* Hydrogen sulfide at high pressure: Change in stoichiometry. *Phys. Rev. B* **93**, 174105 (1–7) (2016)
- [20] Laniel, D. *et al.* Novel sulfur hydrides synthesized at extreme conditions. *Phys. Rev. B* **102**, 134109 (2020)
- [21] Akashi, R., Kawamura, M., Tsuneyuki, S., Nomura, Y. & Arita, R. First-principles study of the pressure and crystal-structure dependences of the superconducting transition temperature in compressed sulfur hydrides. *Phys. Rev. B* **91** (22), 224513 (1–7) (2015)
- [22] Errea, I. *et al.* Hydrogen sulphide at high pressure: A strongly-anharmonic phonon-mediated superconductor. *Phys. Rev. Lett.* **114**, 157004 (1–5) (2015)
- [23] Li, Y. *et al.* Dissociation products and structures of solid H_2S at strong compression. *Phys. Rev. B* **93** (2), 020103(R) (1–5) (2016)
- [24] Ishikawa, T. *et al.* Superconducting H_5S_2 phase in sulfur-hydrogen system under high-pressure. *Sci. Rep.* **6**, 23160 (1–8) (2016)
- [25] Akashi, R., Sano, W., Arita, R. & Tsuneyuki, S. Possible “magneli” phases and self-alloying in the superconducting sulfur hydride. *Phys. Rev. Lett.* **117**, 075503 (1–6) (2016)
- [26] Gordon, E. E. *et al.* Structure and composition of the 200 k-superconducting phase of H_2S at ultrahigh pressure: The perovskite $(\text{SH}^-)(\text{H}_3\text{S}^+)$. *Angew. Chem. Int. Ed.* **55** (11), 3682–3684 (2016)
- [27] Majumdar, A., Tse, J. S. & Yao, Y. Modulated structure calculated for superconducting hydrogen sulfide. *Angew. Chem. Int. Ed.* **56**, 11390–11393 (2017)
- [28] Majumdar, A., Tse, J. S. & Yao, Y. Mechanism for the structural transformation to the modulated superconducting phase of compressed hydrogen sulfide. *Sci. Rep.* **9**, 5023 (2019)

- [29] Verma, A. K. & Modak, P. A unique metallic phase of H₃S at high-pressure: Sulfur in three different local environments. *Phys. Chem. Chem. Phys.* **20**, 26344–26350 (2018)
- [30] Errea, I. *et al.* Quantum hydrogen-bond symmetrization in the superconducting hydrogen sulfide system. *Nature* **532**, 81–84 (2016)
- [31] Bianco, R., Errea, I., Calandra, M. & Mauri, F. High-pressure phase diagram of hydrogen and deuterium sulfides from first principles: Structural and vibrational properties including quantum and anharmonic effects. *Phys. Rev. B* **97**, 214101 (2018)
- [32] Liu, C. *et al.* Strain-induced modulations of electronic structure and electron-phonon coupling in dense H₃S. *Phys. Chem. Chem. Phys.* **20**, 5952–5957 (2018)
- [33] Cui, W. *et al.* Route to high-T_c superconductivity via CH₄ intercalated H₃S hydride perovskites. *Phys. Rev. B* **101**, 134504 (2020)
- [34] Sun, Y. *et al.* Computational discovery of a dynamically stable cubic SH₃-like high-temperature superconductor at 100 GPa via CH₄ intercalation. *Phys. Rev. B* **101**, 174102 (2020)
- [35] Ge, Y., Zhang, F., Dias, R. P., Hemley, R. J. & Yao, Y. Hole-doped room-temperature superconductivity in H₃S_{1-x}Z_x (Z=C, Si). *Mater. Today Phys.* **15**, 100330 (2020)
- [36] Hu, S., Paul, R., Karasiev, V. & Dias, R. Carbon-doped sulfur hydrides as room-temperature superconductors at 270 GPa. *arXiv preprint arXiv:2012.10259* (2020)
- [37] Quan, Y. & Pickett, W. E. Van Hove singularities and spectral smearing in high-temperature superconducting H₃S. *Phys. Rev. B* **93** (10), 104526 (2016)
- [38] Sano, W., Koretsune, T., Tadano, T., Akashi, R. & Arita, R. Effect of van Hove singularities on high-T_c superconductivity in H₃S. *Phys. Rev. B* **93** (9), 094525 (2016)
- [39] Ortenzi, L., Cappelluti, E. & Pietronero, L. Band structure and electron-phonon coupling in H₃S: A tight-binding model. *Phys. Rev. B* **94**, 064507 (2016)
- [40] Akashi, R. Archetypical “push the band critical point” mechanism for peaking of the density of states in three dimensional crystals: Theory and case study of cubic H₃S. *Phys. Rev. B* **101**, 075126 (2020)
- [41] Wang, T. *et al.* Absence of conventional room temperature superconductivity at high pressure in carbon doped H₃S. *arXiv preprint arXiv:2104.03710* (2021)
- [42] Guan, H. & Liu, H. Superconductivity of light-elements doped H₃S. *arXiv preprint arXiv:2108.09437* (2021)
- [43] Müller, P. C., Ertural, C., Hempelmann, J. & Dronskowski, R. Crystal orbital bond index: Covalent bond orders in solids. *J. Phys. Chem. C* **125** (14), 7959–7970 (2021)

- [44] Hoffmann, R. The theoretical design of novel stabilized systems. *Pure Appl. Chem.* **28** (2-3), 181–194 (1971)
- [45] Hoffmann, R., Alder, R. W. & Wilcox Jr, C. F. Planar tetracoordinate carbon. *J. Am. Chem. Soc.* **92** (16), 4992–4993 (1970)
- [46] Olah, G. A. & Rasul, G. From kekule’s tetravalent methane to five-, six-, and seven-coordinated protonated methanes. *Acc. Chem. Res.* **30**, 245–250 (1997)
- [47] Olah, G. A., Prakash, G. K. S., Williams, R. E., Field, L. D. & Wade, K. (eds) *Hypercarbon Chemistry* (John Wiley & Sons, New York, 1987)
- [48] Fahy, S. & Louie, S. G. High-pressure structural and electronic properties of carbon. *Phys. Rev. B* **36**, 36 (1987)
- [49] Martinez-Canales, M. & Pickard, C. J. Thermodynamically stable phases of carbon at multiterapascall pressures. *Phys. Rev. Lett.* **108**, 045704 (2012)
- [50] Daviau, K. & Lee, K. K. M. Zinc-blende to rocksalt transition in sic in a laser-heated diamond-anvil cell. *Phys. Rev. B* **95**, 134108 (2017)
- [51] Hatch, D. M. *et al.* Bilayer sliding mechanism for the zinc-blende to rocksalt transition in SiC. *Phys. Rev. B* **71**, 184109 (2005)
- [52] Gao, G., Liang, X., Ashcroft, N. W. & Hoffmann, R. Potential semiconducting and superconducting metastable Si₃C structures under pressure. *Chem. Mater.* **30**, 421 (2018)
- [53] Marx, D. & Parrinello, M. Structural quantum effects and three-centre two-electron bonding in CH₅⁺. *Nature* **375**, 216–218 (1995)
- [54] Lammertsma, K. & Olah, G. A. Diprotonated methane, CH₆²⁺, and diprotonated ethane, C₂H₈²⁺. *J. Am. Chem. Soc.* **104**, 6851–6852 (1982)
- [55] Lammertsma, K. *et al.* Structure and stability of diprotonated methane, CH₆²⁺. *J. Am. Chem. Soc.* **105**, 5258–5263 (1983)
- [56] Feng, J. *et al.* Structures and potential superconductivity in SiH₄ at high pressure: En route to “metallic hydrogen”. *Phys. Rev. Lett.* **96**, 017006 (1–4) (2006)
- [57] Martinez-Canales, M., Pickard, C. J. & Needs, R. J. Thermodynamically stable phases of carbon at multiterapascall pressures. *Phys. Rev. Lett.* **108** (4), 045704 (2012)
- [58] Liu, H., Zhu, L., Cui, W. & Ma, Y. Room-temperature structures of solid hydrogen at high pressures. *J. Chem. Phys.* **137**, 074501 (1–7) (2012)
- [59] Sun, W. *et al.* The thermodynamic scale of inorganic crystalline metastability. *Sci. Adv.* **2**, e1600225 (2016)

- [60] Allen, P. B. & Dynes, R. C. Transition temperature of strong-coupled superconductors reanalyzed. *Phys. Rev. B* **12** (3), 905 (1975)
- [61] Perdew, J. P., Burke, K. & Ernzerhof, M. Generalized gradient approximation made simple. *Phys. Rev. Lett.* **77** (18), 3865 (1996)
- [62] Kresse, G. & Furthmüller, J. Efficient iterative schemes for *Ab Initio* total-energy calculations using a plane-wave basis set. *Phys. Rev. B* **54** (16), 11169 (1996)
- [63] Blöchl, P. E. Projector augmented-wave method. *Phys. Rev. B* **50** (24), 17953 (1994)
- [64] Dronskowski, R. & Blöchl, P. E. Crystal orbital hamilton populations (COHP): Energy-resolved visualization of chemical bonding in solids based on density-functional calculations. *J. Phys. Chem.* **97** (33), 8617–8624 (1993)
- [65] Maintz, S., Deringer, V. L., Tchougréeff, A. L. & Dronskowski, R. Analytic projection from plane-wave and paw wavefunctions and application to chemical-bonding analysis in solids. *J. Comput. Chem.* **34** (29), 2557–2567 (2013)
- [66] Togo, A., Oba, F. & Tanaka, I. First-principles calculations of the ferroelastic transition between rutile-type and CaCl₂-type SiO₂ at high pressures. *Phys. Rev. B* **78** (13), 134106 (2008)
- [67] Yannello, V. J., Lu, E. & Fredrickson, D. C. At the limits of isolobal bonding: π -based covalent magnetism in Mn₂Hg₅. *Inorg. Chem.* **59**, 12304–12313 (2020)
- [68] Giannozzi, P. *et al.* Quantum espresso: A modular and open-source software project for quantum simulations of materials. *J. Phys. Condens. Matter.* **21** (39), 395502 (2009)
- [69] Dal Corso, A. Pseudopotentials periodic table: From H to Pu. *Comput. Mater. Sci.* **95**, 337–350 (2014)
- [70] Eliashberg, G. M. Interactions between electrons and lattice vibrations in a superconductor. *Sov. Phys. JETP* **11** (3), 696–702 (1960)

Data availability

The data supporting this publication are available from the authors upon reasonable request.

Acknowledgments

We acknowledge support from the U.S. National Science Foundation (DMR-1827815 to E.Z. and DMR-1933622 to R.J.H). This research was also supported by the U.S. Department of Energy (DOE), Office of Science, Fusion Energy Sciences under Award No. DE-SC0020340 and DOE, National Nuclear Security Administration, through the Chicago/DOE Alliance Center under Cooperative Agreement Grant No. DE-NA0003975. Computations were carried out at the Center for Computational Research at the University at Buffalo (<http://hdl.handle.net/10477/79221>).

Author contributions

R.J.H. and E.Z. conceived the project. X.W., T.B., K.P.H., and A.L. carried out the DFT calculations. All authors were involved in data analysis and results discussions. X.W., E.Z. and R.J.H. wrote the manuscript, with contributions from K.P.H.

Additional information

Supplementary Information accompanies this paper at <https://doi.org/xxx/aaa-bbb.ccc>

Competing interests

The authors declare that no competing interests.